13

Influence of ammoniou iodide precursor on the structures and lifetime of charge carriers in the lead sulfide photosensitive elements

© K.S. Makaruk,[1,2] B.N. Miroshnikov,[1] A.D. Barinov,[1] A.I. Popov,[1] I.N. Miroshnikova,[1]
T.D. Patsaev,[3] A.L. Vasiliev,[3] A.V. Goryachev,[2] L.N. Maskaeva[4,5]

[1] National Research University „Moscow Power Engineering Institute“, Moscow, Russia
[2] Institute of Nanotechnology of Microelectronics, Russian Academy of Sciences, Moscow, Russia
[3] National Research Center „Kurchatov Institute“, Moscow, Russia
[4] Ural Federal University after the first President of Russia B.N. Yeltsin, Yekaterinburg, Russia
[5] Ural Institute of State Fire Service of EMERCOM of Russia, Yekaterinburg, Russia
e-mail: MiroshnikovaIN@mpei.ru

Received July 14, 2025
Revised October 23, 2025
Accepted November 13, 2025

The structure and characteristics of photosensitive elements based on thin films of lead sulfide (PbS) were studied. The films were prepared by chemical precipitation in the presence of a precursor (ammonium iodide (NH_4I)) in different molar concentrations. It has been established that iodine and its compounds (formed at an early stage of thin film deposition) lead to a change in the formation mechanism of the material structure. In turn, this leads to a decrease in the thickness of the oxygen-containing layers between the crystallites and has a decisive influence on the increase in the mobility of charge carriers. It is shown that the increase in photosensitivity at low frequencies (up to 800 Hz) is associated with the formation of oxygen-containing compositions and the appearance of a second group of charge carriers with lifetimes of $860-930\,\mu$s.

Keywords: thin films, structure, lead sulfide, chemical deposition method, photosensitive elements, photoelectric parameters, relaxation time.

DOI: 10.61011/TP.2026.03.63169.181-25

Introduction

Lead sulfide (PbS) is a representative of a widespread family of $A^{IV}B^{VI}$ compounds and a direct-band-gap semiconductor material with a band gap of 0.4 eV at 300 K. The compound of interest has a NaCl type (mineral salt) face-centered cubic structure, space group $Fm\overline{3}m$. The lattice parameter is 5.94 Å [1]. This material is used for producing photosensitive elements (PSE) in electrooptical systems (EOS) operated in the IR region from 1 to $3\,\mu$m [2–4], however, due to a high concentration of both types of charge carriers in single crystals, the time constant that defines the sensitivity of these PSE was low (from $6 \cdot 10^{-10}$ to $9 \cdot 10^{-6}$ according to Moss's studies [5]). Techniques for formation of oxygen-rich polycrystalline photosensitive PbS-based thin films has been developed since the 1960s PbS forms p-type traps, thus increasing the hole lifetime and the sensitivity.

In recent years, nanostructured PbS thin films are also used as visible light detectors [6]. Lead sulfide is also a promising material for formation of heterostructures used to create high-efficiency solar cells [7–10], sensors for detecting various gases [11–13] and non-ferrous metal ions in aqueous media [14,15], highly selective sensors for detecting toxic compounds in air [16,17] and for producing quantum dots [18].

One of the essential stages of high-sensitivity element formation process is sensitization, i.e. intentional introduction of oxygen into the PbS lattice as an isoelectronic impurity with high electronegativity. For this, high-temperature annealing in air [19] or two-stage annealing first in oxygen and then in nitrogen [20] are used. Besides annealing, oxygen can be introduced into the crystal structure during chemical deposition from a reaction bath containing, apart from the main components, additional oxidizers (H_2O_2, $K_2S_2O_8$) [18,21,22], reducers (Na_2SO_3, $N_2H_4 \cdot H_2O$, $NH_2OH \cdot HCl$, $Na_2S_2O_3$) [22–25] or activators in the form of various metal salts (silver, mercury, calcium, cadmium, iron (II), gallium and magnesium) [27–30].

In accordance with the Pb-S phase diagram, lead sulfide has surplus of lead atoms with respect to sulfur [18] and, therefore, is an *n*-type semiconductor.

Sensitization of PbS films by both oxygen and iodine is accompanied by a change in the conductivity type (from *n*-type to *p*-type), increase in the concentration of quasi-free holes due to localization of electrons on p-type centers (traps) energetically positioned within the PbS band gap [31,32], while the hole lifetime is growing.

It is known [33,34] that the main parameters of electrooptical systems are voltage sensitivity:

$$S_U = \frac{U_S}{\Phi_E} = \frac{S_{U_0}}{\sqrt{1 + (\omega \cdot \tau)^2}} \tag{1}$$

and specific detectivity:

$$D^* = \frac{U_S \sqrt{A_{EFF} \cdot \Delta f}}{\Phi_E \cdot U_N} = \frac{S_{U_0} \sqrt{A_{EFF} \cdot \Delta f}}{U_N}, \tag{2}$$

where U_S is the rms photoelectric signal voltage; Φ_E is the effective radiation power; $\omega = 2\pi f$ is the cyclic frequency; τ is the photoresist (PR) time constant (equivalent to the majority carrier lifetime); S_{U_0} is the sensitivity at low radiation modulation frequency; $A_{EFF} = l \cdot b$ (l is the distance between PSE contacts, b is the PSE contact width) is the effective PSE area; Δf is the equivalent bandwidth of an amplifier; U_N is the rms noise voltage. $\sqrt{1 + (\omega \cdot \tau)^2}$ reflects a decrease in sensitivity as the signal frequency grows.

It is reasonable that for comparing PSEs having different dimensions and bias voltages, the given parameters are used or values in arbitrary units are considered. For example, S_U^* is the specific (reduced) voltage sensitivity calculated using the following equation [33,35]:

$$S_U^*(\lambda) = \frac{U_S \cdot A_{EFF}}{\Phi_E \cdot U_{PSE}\sqrt{1+\omega^2\tau^2}} \propto \frac{S_{U_0}^*}{\sqrt{1+\omega^2\tau^2}} \propto \frac{\Delta\sigma}{\sigma_0 \cdot \Phi_E} \propto \frac{\eta(\lambda)\cdot\tau}{p \cdot d \cdot \sqrt{1+\omega^2\tau^2}}, \quad (3)$$

where U_{PSE} is the PSE voltage; d is the photosensitive layer thickness; $\eta(\lambda)$ is the wavelength-dependent quantum efficiency of absorbed radiation. EOS designed for control over objects with small angular dimensions use conversion of pulse signals generated during scanning of the environment. $\Delta\sigma/(\sigma_0 \cdot \Phi_E)$ — photoconductivity related to dark conductivity (σ_0) and effective radiation power with fixed modulation frequency, rather than conductivity (photoconductivity — $\Delta\sigma$) increment, serves as a sensitivity criterion for them. Dark conductivity is defined by the concentration of charge carriers in steady state:

$$\sigma_0 = q(n_0 \cdot \mu_n + p_0 \cdot \mu_p), \quad (4)$$

where q is the electron charge; μ_n, μ_p is the electron and hole mobility, respectively; n_0, p_0 are the carrier concentrations in thermodynamic equilibrium state.

Concentration of majority carriers $p = p_1 + p_2$ includes two components: p_1 is caused by oxygen penetration into the volume of PbS crystallites at the sensitization stage, and p_2 is generated by formation of attachment levels on the surface of crystallites formed by oxygen-containing impurities (OCI) [33,36]. With $p_2 > p_1$, which is observed in serial PSE, τ is linearly related to p_2 ($\tau = C \cdot p_2$, where C is the coefficient, whose value is determined experimentally). Thus, the voltage sensitivity values are defined by the ratio of the time constant to the concentration of majority carriers τ/p.

To increase photosensitivity of thin films in low-frequency range, increase the majority carrier lifetime (more often of holes) that coincides with the photoconductivity relaxation time, or decrease the concentration of equilibrium charge carriers, or rather decrease the dark conductivity. Whilst a change in charge carrier mobility in polycrystalline PbS films is generally not considered.

It was reported in [33,36] that a vast majority of commercial IR detectors produced before the early 21st century that are made on the basis of PbS films deposited from reaction baths with addition of various oxidizers, reducers and activators have the main specifications in the following ranges:

- time constant from 50 to 600 μs;
- dark resistance, R_D — from 50 to 400 kΩ;
- sensitivity at the spectral response curve maximum $S_{U\lambda_{\max}}$=(1−400) $\cdot 10^4$ V/W with $\lambda_{\max}$=2.4 μm and integral sensitivity S_U = (1000−3000) V/W;
- specific detectivity at the spectral response curve maximum $D^*_{\lambda_{\max}} = (2.5{-}40) \cdot 10^{10}\,\mathrm{W}^{-1} \cdot \mathrm{cm} \cdot \mathrm{Hz}^{1/2}$ (at room temperature and field-of-vision angle 60°) with theoretical value $D^*_{\lambda_{\max}} = 5.8 \cdot 10^{12}\,\mathrm{W}^{-1} \cdot \mathrm{cm} \cdot \mathrm{Hz}^{1/2}$;
- integral specific detectivity $D^*_{293} \approx (0.7{-}10) \cdot 10^{10}\,\mathrm{W}^{-1} \cdot \mathrm{cm} \cdot \mathrm{Hz}^{1/2}$.

Recently, new modifications of previously known techniques have appeared and can be used to vary photovoltaic parameters. Thus, for example, the chemical bath deposition (CBD) technique allows variation of photovoltaic parameters through introducing various precursors in the reaction bath, and thin film properties will depend on the deposition process duration, concentration of reagents, solution temperature and pH [37–39].

In [26], the researchers discovered an inhibiting effect of $Na_2S_2O_3$ on the process rate due to formation of a stable $Pb(S_2O_3)_3^{4-}$ complex in the reaction bath, and in [40], NH_4Ac was additionally introduced to maintain constant pH in the reaction bath. Unfortunately, in [41], the authors avoid the question related to the presence of oxygen in PbS film, which certainly shall be present because aqueous solutions, besides a reducer in the form of KBr, also contain an oxygen-containing impurity — Na_2SO_3, to ensure high photoconductivity of PbS films.

The use of halogens in producing lead chalcogenide PSE was discussed in the foreign literature much less frequently, however, since as early as the late 1950s [42], it has been known that halogen-containing compounds could control oxygen penetration into thin-film structure microcrystallites. The use of halogens for chemical deposition was probably first discussed in [43], where formation of poorly soluble compounds and complexes was reported. The effect of iodine and other halogens on structure parameters was discussed in more detail for PbSe. In [44], it was discovered that iodine doping of chemically deposited films led to formation of several oxide phases such as PbI_2O_2, Pb_2O_4, and PbI_2. Some other papers also reported that addition of halogen-containing compounds allowed controlling oxygen atom inclusion in the lattice during chemical deposition of structures. Such data were not obtained for lead sulfide structures.

According to the authors of [45], halogens having seven electrons in the outermost electron shell shall have a deep donor effect, therefore it could be suggested that halogen doping of lead sulfide will provide samples with a concentration of electrons of about $10^{20}\,\mathrm{cm}^{-3}$. The

importance of investigating halogen doping of lead sulfide is emphasized by the authors of [46]. A little later, it was reported that halide ions were used as dopants for chemical deposition of PbS films [43–44,47]. In [43], kinetics of chemical deposition of lead sulfide in the presence of ammonium halides in the reaction bath was explored, but photosensitive properties of ammonium halides were scarcely discussed. Further papers [44,47] report that PbS thin films have a sensitivity up to 1200 V/W and a detectivity up to $10^{11}\,\mathrm{cm}\cdot\mathrm{Hz}^{1/2}\cdot\mathrm{W}^{-1}$. It is also shown that dopants can be ranked as $NH_4I > NH_4Cl \geq NH_4Br$ by their sensitizing action. In addition, when any ammonium halide was introduced in the reaction bath, the type of conductivity of PbS changed from *n* to *p*. To explain photosensitive properties of PbS films, the authors of [48] used a self-compensation phenomenon inherent in lead chalcogenides during halogen doping [45], but quantitative interpretation of this phenomenon is currently unavailable. Self-compensating mechanism in PbS films during iodine doping is probably implemented due to formation of point defects in the form of interstitial impurity in the interstitial space and to creation of iodide ion and lead complexes, „Pb-I_2“, that actually provide a lead vacancy. Lines belonging to iodine-/oxygen-containing compounds (PbI_2, $PbSO_4$, PbO) were detected on the Raman scattering spectra of the PbS of interest in the stretching frequency range of $50-1200\,\mathrm{cm}^{-1}$ [49].

In [50], its was discovered that the composition and type of conductivity determined by the sign of thermal emf when forming a temperature gradient in the contact region for films deposited from the reaction bath containing 0.15 mol/l ammonium iodide depended on the deposition process time:

- at a synthesis time of 20 min, the maximum amount of iodine was reported — (9.4 ± 1.0) at.% ([Pb]/[S]= (45.4 ± 1.3) at.%/(45.2 ± 0.6) at.%), films demonstrated the *n*-type conductivity;
- at a synthesis time of 40 min, the amount of iodine was (5.8 ± 0.6) at.% ([Pb]/[S] = (49.1 ± 0.6) at.%/(45.1 ± 0.4) at.%); at this and longer synthesis times, films demonstrated the *p*-type conductivity;
- at a synthesis time of 60 min, the amount of iodine was (5.3 ± 0.4) at.% ([Pb]/[S] = (49.9 ± 0.4) at.%/(44.8 ± 0.3) at.%);
- at a synthesis time of 90 min, the amount of iodine was (2.7 ± 0.3) at.% ([Pb]/[S]= (50.1 ± 0.3) at.%/$(47.2 \pm 0.3$ at.%);

Thus, the highest atomic concentration of iodine is observed after 20 min of synthesis and is (9.4 ± 1.0) at.%. As the deposition time increases, the type of conductivity of the structure changes (from the *n*-type to the *p*-type), the iodine concentration decreases.

Iodine introduction into the PbS thin film structure is an important topic of discussion, as this process allows changing the main properties of photosensitive structures for particular EOSs. The aim of this work was to identify the physical causes of high sensitivity of PSE , when using the ammonium iodide precursor(NH_4I), and the correlation between photovoltaic properties and composition, charge carrier lifetime and morphology.

1. Objects and method of investigation

The objects of investigation were PbS thin films synthesized by chemical deposition from an ammonia-citric reaction bath containing 0.04 mol/l of $Pb(CH_3COO)_2$, 0.3 mol/l of Na3C6H5O7, 4.0 mol/l of NH_4OH and 0.58 mol/l of N_2H_4CS (source of sulfide ions) with the concentration of NH_4I varied from 0.125 to 0.20 mol/l [50]. Films were deposited during 90 min at 353 K in sealed molybdenum glass reactors where degreased microscope slide substrates (72.2 % SiO_2, 14.3 % Na_2O; 1.2 % K_2O, 6.4 % CaO, 4.3 % MgO, 1.2 % Al_2O_3, 0.03 % Fe_2O_3, 0.3 % SO_3) secured in PTFE fixtures were immersed [51]. The reactors were placed in the TS-TB-10 thermostat with a temperature control accuracy of ±0.1 K. After completion of the synthesis, the films were rinsed with distilled water and dried in air.

For comparison, PbS films were deposited from a reaction mixture containing (besides the main components $(NH_2)_2\cdot CS$, $Pb(CH_3COO)_2$)) an oxidizer ($Na_2S_2O_4$ or Na_2SO_3) and a reducer ($H_2NH_2\cdot H_2O$) or (KOH) [19,31,32].

Photovoltaic properties were studied on samples with ohmic nickel contacts. Measurements were performed in accordance with GOST 17772-89 using the K54.410 system with a blackbody (BB) radiation source $T = 573$ K. BB temperature maintenance accuracy was 0. K. Irradiance in the instrument plane was $3\cdot10^{-4}\,\mathrm{W/cm}^2$. Radiation modulator in the form of a perforated disk provided a modulation frequency of 400 Hz, 800 Hz and 1200 Hz. Measurement path bandwidth is 156 Hz, 156 Hz and 189 Hz, respectively. Photoconductive response was recorded as a voltage drop across the matched load resistance. Measurement conditions: radiation source — BB with a temperature of 573 K; bias voltage — 20 V, 30 V and 40 V, ambient temperature — 20 °C – 25 °C. Measurement error of the K54.410 system is about 10 % of the measured variable.

Photoconductivity relaxation time constant τ (majority carrier lifetime) was determined by signal values at 400 Hz and 800 Hz, 800 Hz and 1200 Hz and was compared with results obtained using the ASEC-03E automated system for measuring electrophysical parameters of semiconductors (Special Design Bureau, Institute of Radio Technologies and Electronics of the Russian Academy of Sciences, Fryazino) by relaxation curves after pulsed illumination by the Unomat B24 LZ24/GN80 flash with a temperature of 5600 K and light pulse time of 0.01 s. Acceptance error limit for measurements using the ASEC-03 is about 0.1ms.

Morphology of film samples was studied by the atomic force microscopy using the probe NanoLaboratory INTEGRA Prima made by NT-MDT (Zelenograd). Scanning was conducted in a semi-contact mode using the NSG01 cantilever (hardness 1.45–15.10 N/m). Crystallite sizes were analyzed using Gwyddion v.2.67.

Effect of chemical composition of iodine-doped PbS thin films on the dark resistance and PSE time constant estimated by the voltage sensitivity decay and photocurrent relaxation

Sample №	$[NH_4I]$, mol/l	[Pb], at.%	[S], at.%	[I], at.%	R_D, kΩ	Time constant τ, μs	
						By sensitivity decay	By photocurrent relaxation
1	0.125	47.78 ± 0.55	50.18 ± 0.56	2.04 ± 0.21	1470	560−130	870 and 340
2	0.170	47.70 ± 0.22	50.95 ± 0.09	1.35 ± 0.25	1100	340−120	930 and 280
3	0.200	46.98 ± 0.38	51.99 ± 0.17	1.03 ± 0.35	157	340−250	860 and 380

Elemental composition of films was studied in five different points (followed by averaging of results) on the surface by electron microprobe analysis using the Vega II SBU scanning-electron microscope (Tescan, Czech Republic) fitted with the Inca x-Act energy-dispersive spectrometer (Oxford Instruments, UK). Accelerating voltage was 10 kV, detector acceptance angle was 15°, working distance was 15 mm, data acquisition time was 60 s.

Depth variation of the film composition was measured using two techniques: Auger analysis with layer-by-layer etching and high-resolution transmission microscopy.

Auger-electron spectroscopy used the JEOL Jamp-9510F microprobe (Japan). Accelerating voltage of primary beam electrons was 10 keV, electron beam current was 33 nA, sample angle with respect to normal to the primary electron beam was 60°, electron beam diameter during profiling was more than 100 μm. Analyzer mode was M4 with constant retarding potential and a relative energy resolution of 0.3 %. Ar atom ion source energy for the profile analysis was 2 keV, the etching angle was 41° with respect to the sample plane.

Transmission electron microscopy samples were prepared by the lift out technique using the Helios Nanolab 600 focused ion beam scanning-electron microscope (Thermo Fisher Scientific, USA). Then the samples were examined using the Osiris microscope (Thermo Fisher Scientific, USA) fitted with a high-angle annular dark-field detector (Fischione, USA) and the Super X X-ray energy-dispersive spectrometer (ChemiSTEM, Bruker, USA) at an accelerating voltage of 200 kV. For the purpose of examination, a platinum layer was preliminary sputtered on the photosensitive elements to avoid surface charging effects.

2. Findings and discussion

Elemental composition of PbS thin films chemically deposited from reaction mixtures with varied concentration of ammonium iodide from 0.125 to 0.200 mol/l was examined by the electron microprobe analysis throughout the surface area. Film samples were tested for concentration of main elements (Pb, S and I). Averaged analysis results for three concentrations of ammonium iodide are shown in the table. The sulfur concentration (50.18 at.%−51.99 at.%) in all films is a little higher than the lead concentration (46.98 at.%−47.78 at.%), i.e. chalcogen-metal ratio is 1.07−1.09. Since dark resistance drift was observed in completed samples, the table gives dark resistances after stabilization. It can be seen from the table that an increase in the concentration of NH_4I in the reaction mixture from 0.125 to 0.200 mol/l caused a decrease in the dark resistance RD by a factor of more than 9. Due to the lead deficiency with respect to the stoichiometric composition, the obtained films have the p-type conductivity.

Charge carrier mobility in iodine-doped PbS thin films was determined from the Hall effect measurements [49]. It was identified that the maximum mobility ($\mu = 32.57\,\mathrm{cm^2/(V{\cdot}s)}$) is achieved with an iodine concentration of 1.2 at.%. This value is much higher than in previously studied samples prepared using oxidizers ($12-16\,\mathrm{cm^2/(V{\cdot}s)}$) [19,31,32], which can exert a significant impact on the PSE dark resistance.

As it follows from equation (3), the specific voltage sensitivity of elements is directly proportional to the carrier lifetime. Photosensitive element relaxation time was estimated by two methods: by the time dependence of photoconductivity relaxation (photocurrent relaxation using the ASEC-03E complex) and by the frequency dependence of voltage sensitivity decay measured using the K54.410 system. According to the literature data [35], sensitivity variation in the measured frequency range (400−1200 Hz) shall be as small as possible (about 10 %). We have observed such dependence earlier on many photoresists made using various techniques, in particular, physical deposition with high-temperature annealing and chemical deposition using oxidizers.

For the batch of iodine-doped PbS film samples of interest, measurements of the voltage sensitivity (signal voltage) vs. radiation modulation frequency carried out on the K54.410 system differ considerably. In particular, decrease in the voltage sensitivity occurred in the frequency range of 400−800 Hz, and its values at 800 Hz and 1200 Hz coincided within the measurement accuracy. By analyzing the obtained data, it is suggested that a sharp drop in the voltage sensitivity with a frequency range up to 800 Hz is caused by the presence of several carrier groups with different lifetimes in these films, which was discussed even by V.S.Vavilov [52].

Signal voltage amplitude (voltage sensitivity) variation in the given frequency range makes it possible to calculate the

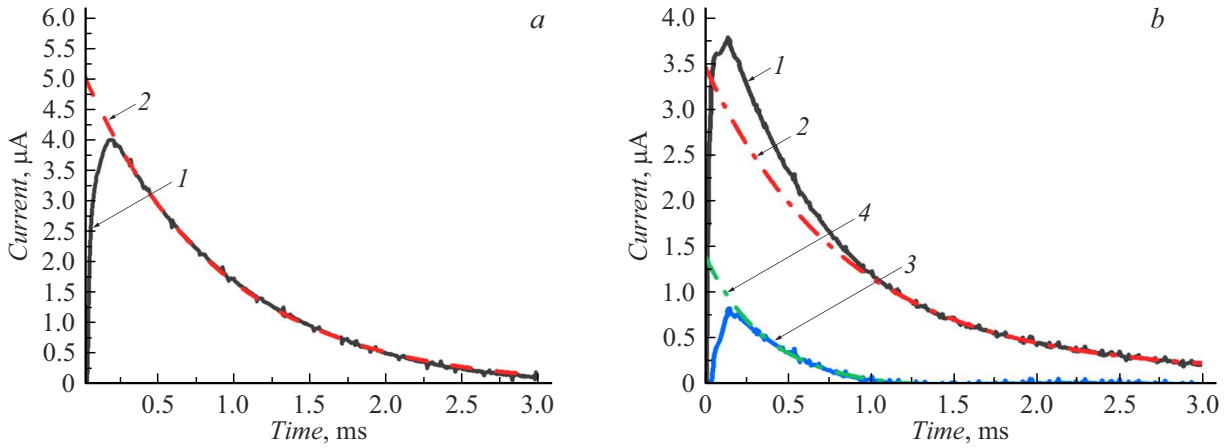

Figure 1. Photocurrent relaxation curves of samples with oxidizer and without NH_4I (*a*) and with ammonium iodide (*b*): *1* — experimental curve; *2* — experiment approximation by the exponential function in the large time region; *3* — difference between curves *1* and *2*; *4* — experiment approximation by the exponential function in the small time region.

relaxation time constant as follows

$$\tau = \sqrt{\frac{(k_0^2 - 1)}{4\pi^2 \cdot (f_2^2 - f_1^2 k_0^2)}}, \qquad (5)$$

where $k_0 = U_{c1}/U_{c2}$, while $U_{c1} > U_{c2}$ at $f_1 < f_2$, U_c is the signal voltage.

Time constants of the test samples calculated by the sensitivity decay are given in the table. It should be noted that PSEs on the basis of PbS films iodine-doped via chemical deposition have the *p*-type conductivity and photosensitivity immediately after deposition, and the time constant can be low — up to 100 μs [49]. Since these photosensitive elements tend to improve their properties in storage (increase the dark resistance, sensitivity and specific detectivity), we measured photovoltaic variables during five months after production. This makes it possible to explain the spread of time constants listed in the table. Analysis of the measurements shows that PSE on the basis of PbS thin films with the highest and lowest iodine concentration in them as estimated by the X-ray spectral microanalysis displays a change in the time constant by more than twice. However, there is no distinct dependence of the time constant on iodine concentration in the films of interest. It should be noted that the used time constant measurement method is not able to estimate reliably the frequency , at which the photoconductivity decay (voltage sensitivity decay) starts, because detailed examination of the 400–800 Hz region is impossible.

In our opinion, the problem of determining the carrier lifetime can be solved by analyzing the photocurrent relaxation curves. Figure 1 shows relaxation characteristics of typical PbS films formed by chemical deposition from a reaction mixture containing either only NH_4I (Figure 1, *b*), or oxidizer (sodium sulfite) (Figure 1, *a*). Relaxation curves were processed using Origin Pro 2021 numerical data analysis package.

It is known that in low light conditions, PSE photoconductivity relaxation is determined by the exponential law. For typical PbS film samples obtained from a reaction bath containing an oxidizer, the relaxation curve is described by one exponent (Figure 1, *a*). At the same time, for a typical PbS sample deposited in the presence of ammonium iodide as shown in Figure 1, *b*, the curve can be described by two exponents with different time constants. The findings can explain the sharp drop in the signal voltage (voltage sensitivity) in the frequency range of 400–800 Hz.

From the above table, it follows that the photoconductivity relaxation time (majority carrier lifetime) constant found by the photocurrent relaxation reflects the lower limit found by the sensitivity decay. Majority carrier lifetimes calculated by the photocurrent relaxation vary in the range from 280 to 930 μs. The spread of time constant values from 50 to 350 μs is typical for all chemically deposited photoresists (for example, FR-202) [33], however, appearance of the second time constant (860–930 μs) can explain high photosensitivity observed in PSE, which agrees with (3).

To identify the origin of the second time constant, focus was made on the morphology and layer-by-layer elemental composition of thin films (PSE). Figure 2 shows $5 \times 5\,\mu$m atomic force microscopy (AFM) surface images for typical test samples and grain size distribution bar charts (insets).

Analysis of the results of thin film surface topology study shows that PbS films chemically deposited in the presence of ammonium iodide (Figure 2, *a*) contain 75 % of grains with a mean size of 100–350 nm and 4 % of nanorange particles, while commercial photoresists made in the presence of oxidizer (Figure 2, *b*) contain larger crystallites (from 600 to 1800 nm). It has been identified that as the iodine concentration increased from 1.03 at.% to 2.04 at.% in PbS films, the arithmetic mean surface roughness Ra decreased from 20.20 nm to 16.93 nm, i.e. the film surface becomes smoother as the iodine concentration in films increases. Grain surface peaks of PSE based on PbS films chemically

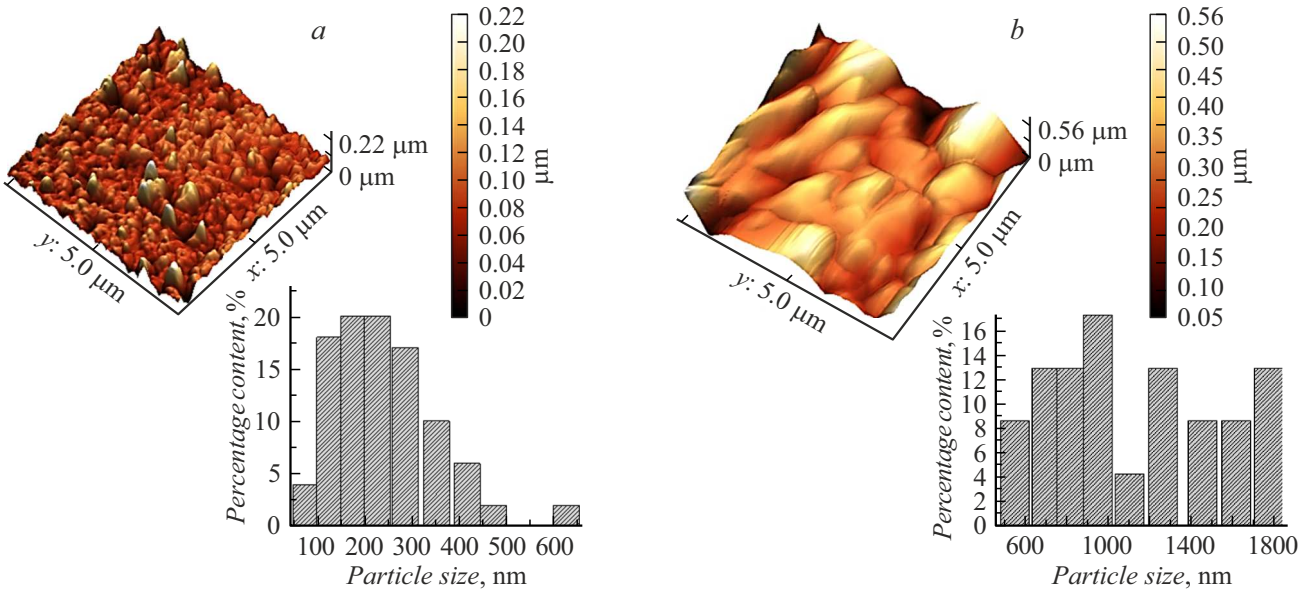

Figure 2. AFM surface images of PSE based on PbS films chemically deposited in the presence of ammonium iodide (№1) (*a*) and Na_2SO_3 oxidizer (*b*). The insets show bar charts of grain size distribution in $5 \times 5\,\mu$m scans.

deposited in the presence of ammonium iodide observed on the AFM images are approximately 2.6 lower than those observed when the oxidizer is used.

In the PSE structures based on iodine-doped lead sulfide, increase in the short-wavelength sensitivity was detected. This increase affects the overall increase in the integral sensitivity due to the presence of nanorange particles in them (Figure 2, *a*). This agrees with results obtained for PbS colloidal quantum dot nanostructures [53].

The next important research stage included investigation of elemental composition variation over the depth of PSE based on PbS films doped either with ammonium iodide or oxidizer.

Electron probe microanalysis provides information from a $600 \times 600\,\mu$m film surface. Another two independent techniques were used for more accurate analysis: transmission electron microscopy (TEM) providing a detailed image of film surface and detailed information concerning the presence of separate atoms, and Auger electron spectroscopy with layer-by-layer etching, thus the element distribution over the sample depth can be built.

Electron microscopy cross-section images of two PSE based on PbS thin films chemically deposited from reaction batch containing, besides the main reagents, the NH_4I additive (*a*) or a typical commercial structure with oxidizer added to the reaction bath (*b*), are shown in Figure 3.

Light shade in Figure 3 corresponds to light-weight elements (these are primarily O and C) and dark shade indicates the presence of heavier elements (S, Pb and Pt). It is important to emphasize that the final cross-section microphotographs are significantly affected by the way in which the sample cross-section was prepared, however, the given images can be considered typical for the groups

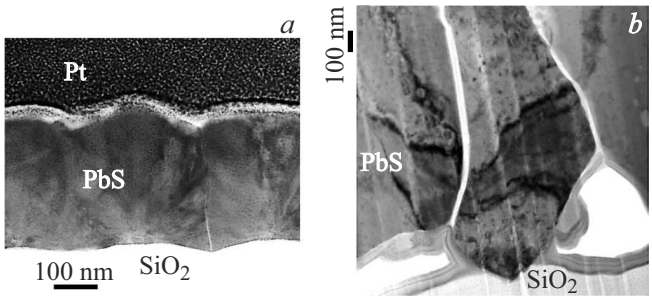

Figure 3. Electron microscopy (TEM) cross-section images of PSE based on PbS films chemically deposited with NH_4I (*a*) or an oxidizer (*b*) added to the reaction bath [30,31].

of film structures of interest. The presence of oxygen-containing impurities detected by high resolution TEM on the crystallite surface of the PbS film samples is caused by oxidation of the crystallites. The presence of oxygen at the film-substrate interface is attributed to formation of $Pb(OH)_2$ crystallization centers, which is proved by the thermodynamic assessment of the boundary conditions of PbS and $Pb(OH)_2$ formation in the used reaction mixture [51].

Lighter areas within the studied structure (Figure 3, *a*) indicate that there are $PbSO_4$, PbO and other oxygen-containing compounds, formation of which during deposition of PbS structures was proved in [50,54]. Note that such oxygen is not necessarily active, i.e. influencing the concentration of holes (as p-type traps) , but introduction of oxygen (isoelectronic acceptor) can lead not only to the impact on the hole lifetime, but also to crystal lattice deformation. Due to a large difference in sizes (atom

radii $a_0 = 60$ (48) pm for oxygen and 127 pm for sulfur with covalent radii of 73 pm and 102 pm, respectively) and electronegativities (3.44 for oxygen and 2.58 for sulfur on the Pauling scale), the O-S pair forms an OS center [55]. Such center implies that new localized levels occur near the bottom of the conduction band, and causes a change in the PbS band structure when the concentration of impurity increases a little. Thus, the equilibrium between anions and cations can still exist, when there is sulfur deficiency, due to oxygen built in the PbS structure.

The main difference in the PbS film PSEs is in the thickness of oxygen-containing interlayers between crystallites. Iodide introduction into the structure presumably changes the film growth process in such a way that oxygen-containing interlayers almost disappear (their thickness is less than 5 nm). Interlayers between crystallites are much thicker (up to 50 nm) in the microphotograph of the typical PbS sample obtained in the presence of oxidizer in the reaction bath (Figure 3, *b*). From the microphotographs of the studied PbS film PSE (with NH_4I), it can be suggested that there are virtually no obstacles in the form of oxide barriers (or they are tunnel-transparent) for passage of majority carriers — holes to contacts, while the concentration of holes related to OCI (p_2) decreases. Thus, there are two opposite processes: decrease in the concentration of majority carriers and increase in the majority carrier mobility. These processes compensate each other, and the sensitivity and specific detectivity grow due to a significant increase in the carrier lifetime.

However, TEM cannot answer the question about iodine localization because charge numbers of iodine ($Z_I = 53$) and lead sulfide ($(Z_s + Z_{Pb})/2 = 49$) are close to each other and therefore are hard to distinguish by the color background on a microphotograph.

For elemental analysis directly on the cross-section, a sample with the highest relative concentration of iodine as shown in the table was selected from the test group. Figure 4 shows the depth variation of the averaged elemental composition and a cross-section microimage (inset) made using the high-angle annular dark-field detector (Z^2-contrast), where lighter shades correspond to heavy elements (colors opposite those shown in Figure 3, *a*; the arrow shows a composition scanning direction).

Consider the characteristics of the distribution of main elements over the sample depth taking into account the spread of percentage content of the main elements (Figure 4). In the platinum layer deposited on the sample surface (from 0 nm to 70–80 nm), a large amount of carbon (about 37 at.%–60 at.%) is observed, which can be caused by contamination of the material or by Pt deposition technique. Partial entry of carbon reaching 10 at.%–12 at.% can occur in the PbS film composition from the reaction bath components, in particular, $Pb(CH_3COO)_2$, $Na_3C_6H5O_8$ and N_2H_4CS.

Stoichiometry between lead and sulfur is not met because the percentage content of lead is higher than that of sulfur: the amount of Pb varies within 42 at.%–56 at.%, and the

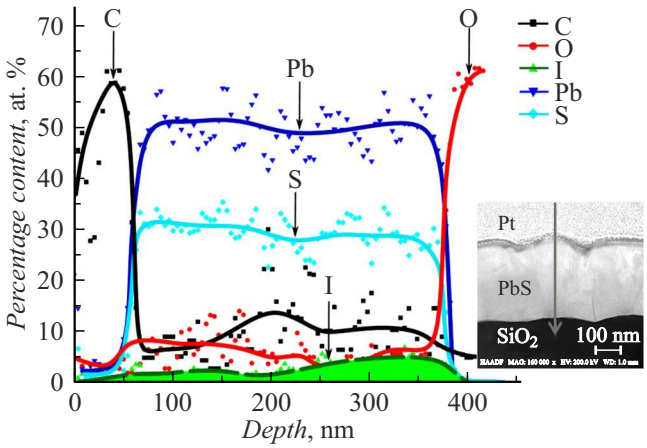

Figure 4. Variation of the elemental composition in depth of the PbS film chemically deposited in the presence of NH_4I.

amount of S varies within 28 at.%–33 at.%. Film thickness is estimated by a sharp increase in the oxygen concentration: for a typical sample from the test group, the growth occurs at a depth of 370 nm from the surface. Thus, if the deposited Pt layer (not shown in Figure 4) is subtracted from the total structure thickness, the film thickness will be approximately 290 nm, which is much smaller than that of typical PbS samples deposited in the presence of oxidizer in the reaction bath.

Special focus shall be made on the distribution and concentration of oxygen and iodine, as noted above, they can have direct effect on the photovoltaic properties of PSE. Thus, oxygen distribution throughout the PbS structure thickness is nonuniform: concentration varies from 2 at.% to 13 at.%. For typical films produced using an oxidizer as a precursor, relative concentration of oxygen is lower than 5 at.%, which is much smaller than that in the PSE of interest. In addition, such films contain the same amount of lead and sulfur — approximately 40 at.%, and the concentration of carbon contaminations is up to 20 at.% [31].

We proceed to discussing the role of iodine in the thin films of interest. As shown in Figure 4, concentration of iodine atoms (color filled) is unsteady over the PSE thickness. For the given sample, iodine concentration is within 1 at.%–3 at.% in the most part of the sample from the surface to the depth of 200 – 240 nm. At a larger depth, its concentration grows up to 4 at.%–6 at.% and remains at this level to the substrate. Thus, iodine-containing compounds are concentrated mainly at the substrate.

Difference in the content of iodine for experimental data obtained from electron microprobe analysis using a scanning-electron microscope and TEM is defined by the level of locality of the used research method. Locality for TEM is small, therefore data in various regions of an individual grain of the structure can be seen. For the scanning-electron microscopy case, the area of study is large and data result from integral information collection over the

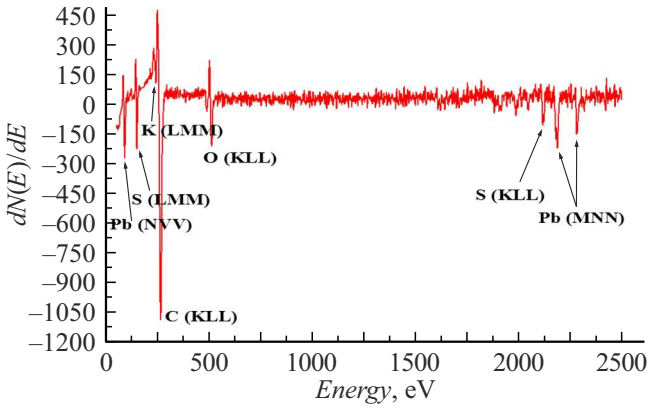

Figure 5. Panoramic Auger spectrum of the photosensitive element surface.

volume of test sample, i.e. the result is averaged between 1 at.%.–3 at.%. and 4 at.%.–6 at.%.

For more detailed study of iodine and oxygen localization in the surface layer and at some depth, the Auger electron spectroscopy method was used. For this study, a sample with the lowest concentration of iodine (according to the electron microprobe analysis results) was taken.

The panoramic spectrum measured on the photosensitive element surface (Figure 5) didn't identify the presence of iodine. A high carbon peak is caused by surface contamination. Such spectrum was observed earlier for samples only with oxidants, i.e. without using NH_4I [56].

Figure 6, *a* shows differential Auger spectra for the test sample after 5 min of etching compared with the iodine spectrum from JEOL database. The obtained experimental peaks in the medium energy region correspond to iodine MNN [57]. It is important to emphasize that they are displayed only after a minute of etching. Analysis of the Auger spectra measured at different etching times made it possible to specify iodine and oxygen distribution over the film depth (Figure 6, *b*).

Analysis in Figure 6, *a* proves that the sensitive layer simultaneously contains both elements (iodine and oxygen), and the highest relative concentration of iodine was about 0.31 at.%.–0.36 at.% during etching in the range from 2.5 to 5.0 min, i.e. at the substrate interface. Thus, the given layer was formed during the first deposition minutes and facilitated the transition from the *n*-type to *p*-type of conductivity. This study method is local. Therefore, there are deviations from the data obtained by the electron microprobe analysis method.

The composition analysis results suggest that iodine-containing compounds are formed mainly at the initial film deposition stage. The data are in agreement with the assumption made in [48] concerning the above-mentioned self-compensation in the studied structures.

Conclusion

The paper provides experimental data for formation of photosensitive elements on the basis of PbS obtained via chemical deposition with varying concentration of ammonium iodide (NH_4I) added as a precursor to the reaction bath. The findings provide new details regarding the possible causes of increasing PSE signal at low frequencies (up to 800 Hz) compared with film structures obtained using only oxidizers (without NH_4I).

It has been identified that the presence of ammonium iodide in the reaction bath led to a decrease in the film thickness, which is undesirable because it reduces the signal in the long-wavelength region („uniform absorption" region throughout the film thickness), but led to an increase in the signal in the short-wavelength region due to an increase in the amount of smaller grains (100–350 nm) up to 75 % and growth of nanoparticle fraction (smaller than 100 nm)

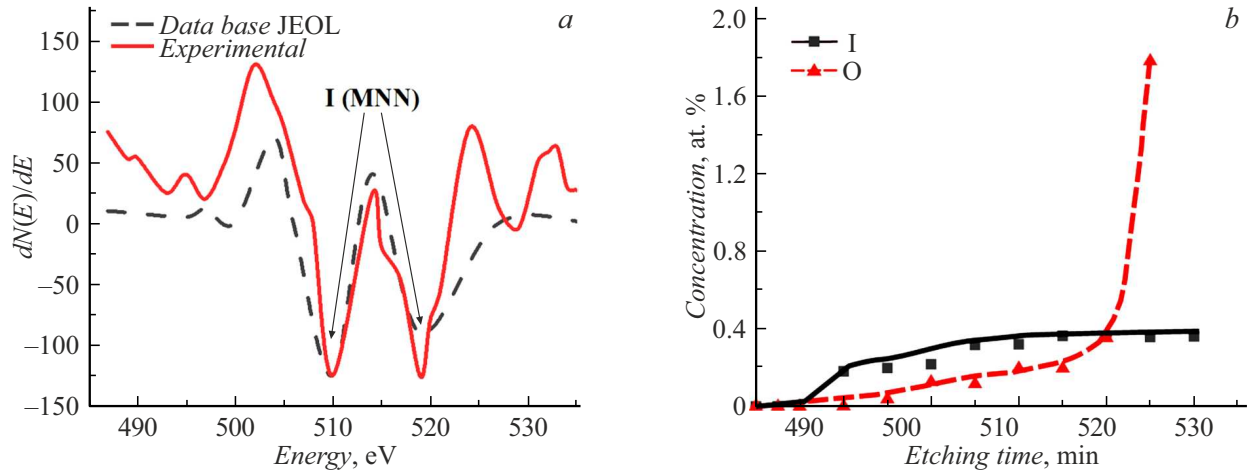

Figure 6. Peaks of differential Auger spectra of iodine MNN after 5 min of etching compared with JEOL database (*a*) and dependence of the iodine and oxygen concentrations over the depth of iodine-doped PbS film on the etching time (*b*).

to 3 % compared with commercial structures obtained when using oxidizers.

High-resolution TEM methods was used to find that due to the presence of iodine in the structure of studied PSE (with NH_4I), there are virtually no OCI between individual crystallites or OCI are tunnel-transparent. Therefore, charge carriers can reach the contacts without changing their path at a constant electric field strength, leading to an increase in mobility compared with typical structures with an oxidizer.

Reduction of OCI at grain boundaries is followed by increase in the oxygen concentration in grains themselves (2 at.%.−13 at.%). Certainly, not all oxygen turns out to be active, but the presence of oxygen can affect both a change in the concentration of free holes (concentration of holes related to OCI (p_2)) and a possible deformation of crystal lattice due to the oxygen that is an isoelectronic impurity and can substitute sulfur atoms. Oxygen built in the lattice is an acceptor, which leads to an increase in the hole lifetime. It has been found that compounds with oxygen and iodine formed in lower film layers (at the initial deposition stage) increase the lifetime of one group of carriers, which agrees well with the appearance of the second time constant registered by the photoconductivity relaxation time.

The provided findings expand the concept of photoconductivity mechanisms for complex polycrystalline structures, which include PbS-based PSE, and allow modification of the chemical process for certain EOS.

Funding

The study was carried out with the financial support of the Ministry of Science and Higher Education of the Russian Federation (topic № FEUZ-2026-0008).

Conflict of interest

The authors declare no conflict of interest.

References

[1] Yu.I. Ravich, B.A. Efimova, I.A. Smirnov. *Metody issledovaniya poluprovodnikov v primenenii k khal'kogenidam svintsa PbTe, PbSe, PbS* (Nauka, M., 1968) (in Russian).
[2] S.I. Sadovnikov, A.I. Gusev. J. Alloys Compounds, **573**, 65 (2013). DOI: 10.1016/j.jallcom.2013.03.290
[3] E. Pentia, V. Draghici, G. Sarau. J. Electrochem. Soc., **151** (11), G729 (2004). DOI: 10.1149/1.1800673
[4] A. Ounissi, N. Ouddai, S. Achour. Eur. Phys. J. Appl. Phys., **37** (3), 241 (2007). DOI: 10.1051/epjap:2007034
[5] T.S. Moss. Proc. Phys. Soc., **B66** (12), 993 (1953). DOI: 10.1088/0370-1301/66/12/301
[6] P.M. Khanzode, D.I. Halge, V.N. Narwade, J.W. Dadge, K.A. Bogle. Optik, **226**, 165933 (2021). DOI: 10.1016/j.ijleo.2020.165933
[7] P.L. Nichols, Z. Liu, L. Yin, S. Turkdogan, F. Fan, C.Z. Ning. Nano Lett., **15** (2), 909 (2015). DOI: 10.1021/nl503640x
[8] J. Hernadez-Borja, Y.V. Vorobiev, R. Ramirez-Bon. Solar Energy Mater. Solar Cells, **95**, 1882 (2011). DOI: 10.1016/j.solmat.2011.02.012
[9] F. Jähnig, D. Bozyigit, O. Yarema, V. Wood. APL Mater., **3**, 020701 (2015). DOI: 10.1063/1.4907158
[10] D.G. Moon, S. Rehan, D.H. Yeon, S.M. Lee, S.J. Park, S. Ahn, Y.S. Cho. Solar Energy Mater. Solar Cells, **200**, 109963 (2019). DOI: 10.1016/j.solmat.2019.109963
[11] X. Chen, J. Hu, P. Chen, M. Yin, F. Meng, Y. Zhang. Sensors and Actuators B: Chemical, **339**, 129902 (2021). DOI: 10.1016/j.snb.2021.129902
[12] V.V. Burungale, R.S. Devan, S.A. Pawar, N.S. Harale, V.L. Patil, V.K. Rao, Yuan-Ron Ma, J.E. Ae, J.H. Kim, P.S. Patil. Mater. Science-Poland, **34** (1), 204 (2016). DOI: 10.1515/msp-2016-0001
[13] T.V. Beatriceveena, E. Prabhu, A. Sree Rama Murthy, V. Jayaraman, K.I. Gnanasekar. Appl. Surface Sci., **456**, 430 (2018). DOI: 10.1016/j.apsusc.2018.06.145
[14] I.V. Zarubin, V.F. Markov, L.N. Maskaeva, N.V. Zarubina, M.V. Kuznetsov. J. Analytical Chem., **72** (3), 327 (2017). DOI: 10.1134/s1061934817030145
[15] T.A. Fatkhetdinova, V.F. Markov, E.A. Zorina, L.N. Maskaeva, I.D. Basalaev. Butlerovskie soobshcheniya, **82** (2), 84 (2025) (in Russian).
[16] T. Blachowicz, A. Ehrmann. Appl. Sci., **10** (5), 1743 (2020). DOI: 10.3390/app10051743
[17] Z. Ren, J. Sun, H. Li, P. Mao, Y. Wei, X. Zhong, J. Hu, S. Yang, J. Wang. Advanced Mater., **29**, (33) 1702055 (2017). DOI: 10.1002/adma.201702055
[18] C. Naşcu, V. Vomir, I. Pop, V. Ionescu, R. Grecu. J. Mater. Sci. Engineering: B, **41** (2), 235 (1996). DOI: 10.1016/S0921-5107(96)01611-X
[19] B.N. Miroshnikov, I.N. Miroshnikova, H.S.H. Mohamed, A.I. Popov. Measurement Techniques, **58** (2), 167 (2015). DOI: 10.1007/s11018-015-0680-8
[20] L. Fan, Z. Huang, Q. Lü, G. Liu, J. Liu. Acta Optica Sinica, **43** (10), 1031001 (2023). DOI: 10.3788/AOS$_2$22038
[21] G.H. Blount, P.J. Schreiber, D.K. Smith, R.T. Yamada. J. Appl. Phys., **44** (3), 978 (1973). DOI: 10.1063/1.1662381
[22] G.M. Wolten. J. Electrochem. Society, **122** (8), 1149 (1975). DOI: 10.1149/1.2134413
[23] Metin Kul. J. Sci. Technology B-Theoretical Sci., **7** (1), 46 (2019). DOI: 10.20290/aubtdb.465445
[24] M. Sasani Ghamsari, M.K. Araghi, S.J. Farahani. Mater. Sci. Engineering: B, **133**, 113 (2006). DOI: 10.1016/j.mseb.2006.06.021
[25] I. Pop, V. Ionescu, C. Naşcu, V. Vomir, R. Grecu, E. Indrea. Thin Solid Films, **283**, 119 (1996).
[26] B. Altıokka. Arabian J. Sci. Engineering, **40** (7), 2085 (2015). DOI: 10.1007/s13369-015-1680-3
[27] H.N. Venkoba Rao, J. Kuppuswamy, R. Lakshmi Naraynan. Indian J. Pure Appl. Phys., **1** (9), 335 (1963).
[28] S.M. Simic, Z.B. Marinkovic. Infrared Phys., **8**, 189 (1968). DOI: 10.1016/0020-0891(68)90008-0
[29] Z.B. Marinkovic, V.M. Simic. J. Infrared Phys., **10**, 187 (1970). DOI: 10.1016/0020-0891(70)90010-2.
[30] L.N. Maskaeva, N.A. Forostyanaya, V.F. Markov, A.S. Eremina, K.A. Karpov. Butlerovskie soobshcheniya, **51** (7), 115 (2017) (in Russian).

[31] H.S.H. Mohamed, M. Abdel-Hafiez, B.N. Miroshnikov, A.D. Barinov, I.N. Miroshnikova. J. Mater. Sci. Semiconductor Processing, **27**, 725 (2014). DOI: 10.1016/J.MSSP.2014.08.010
[32] B.N. Miroshnikov, I.N. Miroshnikova, A.I. Popov, M.Y. Zinchenko. J. Nanoelectron. Optoelectron, **9**, 783 (2014). DOI: 10.1166/jno.2014.1677
[33] B.N. Miroshnikov, I.N. Miroshnikova, A.I. Popov. FTP, **52** (2), 243 (2018) (in Russian). DOI: 10.21883/FTP.2018.02.45450.8639 [B.N. Miroshnikov, I.N. Miroshnikova, A.I. Popov. Semiconductors, **52** (2), 231 (2018). DOI: 10.1134/S1063782618020082]
[34] Y.H. Mohammed Thabit, N.M. Kaawash, Ir.H. Devidas, M.S.K. Nabeel. J. Phys.: Conf. Ser., **2426** (1), 012004 (2023). DOI: 10.1088/1742-6596/2426/1/012004
[35] M.D. Aksenenko, E.A. Krasovsky. *Fotorezistory* (Sovetskoe radio, M., 1973) (in Russian)
[36] V.G. Butkevich, E.R. Globus, L.N. Zalevskaya. (in Russian) Prikladnaya fizika, **2**, 52 (1999) (in Russian).
[37] B. Altıokka, M. Önal. J. Optoelectronics and Advanced Mater., **25**, 42 (2023).
[38] Ali M. Mousa, Sima M. Hassen, S. Mohmoed. International Lett. Chem., Phys. Astronomy, **34**, 1 (2014). DOI: 10.56431/p-x3182s
[39] A.N. Chattarki, S.S. Kamble, L.P. Deshmukh. Mater. Lett., **67** (1), 39 (2012). DOI: 10.1016/j.matlet.2011.08.10
[40] B. Abdallah, R. Hussein, N. Al-Kafri, W. Zetoun. Iranian J. Sci. Technol., Transactions A: Sci., **43**, 1371 (2019). DOI: 10.1007/s40995-019-00698-1
[41] E.M. Larramendi, O. Calzadilla, A. Gonzalez-Arias, E. Hernandez, J. Ruiz-Garcia. Thin Solid Films, **389**, 301 (2001). DOI: 10.1016/S0040-6090(01)00815-X
[42] J.N. Humphrey, W.W. Scanlon. Phys. Rev., **105** (2), 469 (1957). DOI: 10.1103/physrev.105.469
[43] V.F. Markov, L.N. Maskaeva, G.A. Kitaev. Inorganic Mater., **36** (7), 657 (2000).
[44] Y. Suh, S.-H. Suh. J. Infrared Sensors, Devices, Applications, **9974**, 997405 (2016). DOI: 10.1117/12.2237284
[45] V.I. Kaidanov, Yu.I. Ravich. UFN, **145** (1), 51 (1985) (in Russian). DOI: 10.3367/UFNr.0145.198501b.0051
[46] S.P. Zimin, R.F. Zaikina. FTP, **29** (4), 729 (1995) (in Russian).
[47] V.F. Markov, A.V. Shnaider, M.P. Mironov, V.F. Diakov, L.N. Maskaeva. Perspektivnye materialy, **3**, 28 (2008) (in Russian).
[48] L.N. Maskaeva, A.V. Beltseva, E.V. Mostovshchikova,V.I. Voronin, O.S. Eltsov, I.V. Baklanova, P.N. Mushnikov, K.S. Makaruk, V.F. Markov. Thin Solid Films, **817**, 140654 (2025). DOI: 10.1016/j.tsf.2025.140654
[49] V.F. Markov, L.N. Maskaeva, E.V. Mostovshchikova, V.I. Voronin, A.V. Pozdin, A.V. Beltseva, I.O. Selyanin, I.V. Baklanova. J. Phys. Chem., **24** (26), 16085 (2022). DOI: 10.1039/d2cp01815b
[50] A.V. Pozdin. *Avtoreferat kand.diss.* (YrFU, Ekaterinburg, 2024) (in Russian).
[51] L.N. Maskaeva, A.V. Beltseva, O.S. Eltsov, I.V. Baklanova, I.A. Mikhailov, V.F. Markov. Opt. i spektr., **131** (10), 1380 (2023) (in Russian). DOI: 10.61011/OS.2023.10.56890.4557-23
[52] V.S. Vavilov. *Deistvie izluchenij na poluprovodniki* (GIFML, M., 1963)
[53] V.S. Popov, V.P. Ponomarenko, D.V. Demkin, I.A. Shuklov, A.V. Gadomskaya, S.B. Brichkin, N.A. Lavrentiev, V.Yu. Gak, A.E. Mirofyanchenko, E.V. Mirofyanchenko. Doklady Rossiiskoi akademii nauk. Fizika, tekhnicheskie nauki, **511** (1), 78 (2023). DOI: 10.31857/S2686740023040120
[54] S. Espevik, W. Chen-ho, R.H. Bube. J. Appl. Phys., **42** (9), 3513 (1971). DOI: 10.1063/1.1660763
[55] N.K. Morozova, B.N. Miroshnikov. Semiconductors, **52** (3), 278 (2018). DOI: 10.1134/S106378261803017X
[56] I.B. Varlashov, P.V. Mitasov, I.N. Miroshnikova, B.N. Miroshnikov, H.S.H. Mokhamed. Vestnik MEI, **2**, 103 (2015) (in Russian).
[57] L.E. Davis, N.C. MacDonald, P.W. Palmberg, G.E. Riach, R.E. Weber. *Handbook of Auger electron spectroscopy*. Second ed. (Physical Electronics Division PerkinElmer Corporation, Eden Prairie, Minn 1976)

Translated by E.Ilyinskaya